Using channeling properties for studying the impact parameter dependence of electron capture by 20 MeV/u uranium ions in a silicon crystal

E. Testa, P.N. Abufager, F. Bosch, A. Brauning-Demain, H. Brauning, M. Chevallier, C. Cohen, D. Dauvergne, A. Gumberidze, A. L'Hoir, et al.

▶ **To cite this version:**

E. Testa, P.N. Abufager, F. Bosch, A. Brauning-Demain, H. Brauning, et al.. Using channeling properties for studying the impact parameter dependence of electron capture by 20 MeV/u uranium ions in a silicon crystal. Physical Review A : Atomic, molecular, and optical physics [1990-2015], 2007, 76, pp.062901. 10.1103/PhysRevA.76.062901 . in2p3-00164198

HAL Id: in2p3-00164198
https://in2p3.hal.science/in2p3-00164198v1

Submitted on 19 Jul 2007

HAL is a multi-disciplinary open access archive for the deposit and dissemination of scientific research documents, whether they are published or not. The documents may come from teaching and research institutions in France or abroad, or from public or private research centers.

L'archive ouverte pluridisciplinaire **HAL**, est destinée au dépôt et à la diffusion de documents scientifiques de niveau recherche, publiés ou non, émanant des établissements d'enseignement et de recherche français ou étrangers, des laboratoires publics ou privés.

Using channeling properties for studying the impact parameter dependence of electron capture by 20 MeV/u uranium ions in a silicon crystal

E. Testa[1], P.N. Abufager[2], F. Bosch[3], A. Braüning-Demian[3], H. Bräuning[4], M. Chevallier[1], C. Cohen[5], D. Dauvergne[1], A. Gumberidze[3], A. L'Hoir[5], R. Kirsch[1], C. Kozhuharov[3], D. Liesen[3], P.H. Mokler[4,5], J.C. Poizat[1], C. Ray[1], R.D. Rivarola[2], J.P. Rozet[6], Th. Stöhlker[3], S. Toleikis[3], M. Toulemonde[7], D. Vernhet[6] and P. Verma[3]

[1]Institut de Physique Nucléaire de Lyon, Université de Lyon, F-69003 Lyon; Université Lyon 1 and IN2P3/CNRS, UMR 5822, F-69622 Villeurbanne, France

[2]Instituto de Fisica Rosario (CONICET-UNR), Av. Pellegrini 250, 2000 Rosario, Argentina

[3]Gesellschaft für Schwerionenforschung (GSI), D-64291 Darmstadt, Germany

[4]Institut für Atom und Molekülphysik, Justus Liebig Universität, D-35392 Giessen, Germany

[5]Max-Planck-Institut für Kernphysik, 69117 Heidelberg, Germany

[6]Institut des Nano-Sciences de Paris, CNRS-UMR75-88, Universités Paris VI et Paris VII, 75251 Paris Cedex 05, France

[7]Centre Interdisciplinaire de Recherche Ions-Lasers, UMR 11 CEA-CNRS, 14040 Caen Cedex, France

Abstract

The impact parameter dependence of electron capture by 20 MeV/u U^{91+} ions has been studied by means of channeling in a 11 µm thick silicon crystal. Such ions are far from their equilibrium charge state in matter, and channeling offers a unique opportunity to study electron capture in conditions going from the extreme case of a single capture event (for the best channeled ions) to the case of multiple charge exchange events leading to the charge state equilibrium (for unchanneled ions). For each incident ion, the charge state at emergence, energy loss, electron emission and X-ray yields are measured. The correlations between these quantities are studied. The data are reproduced by simulations based on the ion flux distribution. We show that the Mechanical Electron Capture (MEC) dominates at impact parameters smaller than 0.5 Å, whereas Radiative Electron Capture (REC) is the only process occurring beyond. Specific features associated to highly charged heavy ions at intermediate velocities are discussed, in particular ionization following capture into highly excited states, and local electron density enhancement due to the electron gas polarization. The measured impact parameter dependence of capture probabilities is compared to CDW-EIS (continuum distorted waves – eikonal initial state) calculations, extrapolated to n>5 final states.

I. Introduction

Fast heavy ions traveling through matter may carry bound electrons if their velocity v is not large compared to the orbital velocity v_K of their K-shell electrons. They suffer atomic collisions that may result in charge exchange processes. For a given projectile velocity the electron capture and loss cross sections vary in opposite ways with the instantaneous ion charge state: the higher the charge state, the higher (lower) the capture (loss) cross section. As a consequence the mean charge state of projectiles penetrating matter tends toward a value for which electron capture and loss cross sections are equal and that is called the equilibrium charge state. The measurement of charge state distributions of ions transmitted through thin

targets [1] in combination with calculation codes [2] has been used since long in order to determine charge exchange cross sections.

In ordinary matter, electron loss is essentially due to Nuclear Impact Ionization (NII), but to some extend also to Electron Impact Ionization (EII); for non-relativistic ions, electron capture is essentially due to the Mechanical Electron Capture (MEC), that involves bound target electrons, whereas the Radiative Electron Capture (REC), that may involve also quasi-free electrons, has much smaller cross sections. The present study is devoted to the impact parameter dependence of electron capture (MEC and REC). The Mechanical Electron Capture is a three-body process of bound electron capture in which energy and momentum are conserved by means of the target atom recoil. For this reason, and also because initial and final wave functions of the transferred electron must overlap both in spatial and momentum spaces, MEC probabilities are expected to be peaked at rather small impact parameters relative to target atoms, and then to decrease according to the size of electronic shells on which electrons are captured.

Contrary to total cross sections, the impact parameter dependence of MEC probabilities cannot be determined directly, because impact parameters of atomic collisions are not observable quantities. Recently the Recoil Ion Momentum Spectroscopy (RIMS) technique [3, 4] has been used successfully for studying those processes in fast ion-atom collision experiments with gas targets. However the use of RIMS for measuring impact parameter distributions is not straightforward because it is necessary to establish the relation between the impact parameter of the collision and the transverse momentum of the recoiling atom and therefore to evaluate the screening of the target nuclear potential. A few experiments have been performed with light ion-target systems ([5] and references therein) for which the above relation is not obscured by the presence of too many electrons.

Another way to control impact parameter distributions is to use channeling conditions in a single crystal [6]. This opportunity has been first demonstrated in the pioneering work of Datz and co-workers presented in ref [7] where the energy loss rate of ions in planar channeling conditions was studied as a function of their distance from atomic planes. Discovered more than forty years ago, ion channeling has been widely studied for decades in all its aspects (for a review, see for instance references [8, 9]). When fast ions enter a single crystal along a major planar or axial direction, they experience strongly correlated binary collisions with target atoms, that repel them from atomic planes or strings. Then the uniform flux of the incident beam becomes rapidly non-uniform as the ions penetrate into the crystal bulk. As a result their interaction with the solid is deeply modified: close nuclear encounters are essentially suppressed and the rate of energy loss is reduced. If the projectiles are heavy ions traversing a thin crystal, their electron capture and loss probabilities are strongly lowered, which completely modifies the charge state distribution of the transmitted projectiles. Our collaboration has already used channeling to study the impact parameter dependence of ionization processes (and thus the competition between NII and EII). In these experiments, the incident ions chosen had a strong electron excess compared to their mean equilibrium charge state in matter [10].

In the present experiment, we use channeling for studying the impact parameter dependence of electron capture. For this purpose, we have chosen nearly bare very heavy incident ions (20 MeV/u H-like U^{91+}) with a very low adiabaticity parameter $\eta=v/v_K$, thus extending previous studies of capture processes with much lighter ions [11, 12]. In our experiment the incident ions have a charge much higher than their mean equilibrium charge state and, as long as the latter is not reached, they mostly experience electron capture. This is the case for channeled projectiles all along their path through thin single crystals: these ions

travel far from atomic cores and their charge exchange probability is highly reduced. The trajectories of these ions in the crystal can be obtained by Monte-Carlo simulations and the corresponding impact parameter distributions with respect to target nuclei can be deduced. Then, by measuring charge state distributions at the crystal exit, we have been able to access with precision to MEC probabilities corresponding to collisions occurring in the 0.2-0.5 Å impact parameter range. In this range the MEC probabilities decrease steeply for increasing impact parameters and we have been able to study precisely this variation. Actually, measuring such MEC probabilities at large impact parameter is essential in order to check whether bare H-like very heavy ions can be transported inside a crystal without charge exchange, which would lead to potential applications at lower energies.

In section II, we describe our experiment and present the measurement of the charge state *Q* and energy of the projectiles transmitted through the crystal, in coincidence with the detection of X-rays and electrons emitted in the ion-crystal interaction. The section III is devoted to the simulations performed to reproduce our experimental data and provide quantitative impact parameter information on the electron capture. In section IV, we discuss our results and compare them to CDW-EIS (Continuum Distorted Waves - Eikonal Initial State) calculations.

II. Experiment

Our experimental set-up and part of our data have already been presented in a previous paper [13]. Briefly, 20 MeV/u H-like U^{91+} ions were extracted from the storage ring ESR at GSI (Darmstadt) and sent onto a 9.6 μm thick (111) silicon crystal fixed on by a three-axis goniometer. The projectiles emerging from the crystal were charge- and energy-analyzed by means of a magnetic spectrometer and collected in a 2D position sensitive detector located at the focal plane of the magnet. The crystal was tilted by about 35.2° to the beam direction (its effective thickness being 11.7 μm), which allowed the crystal alignment along the <110> direction. The crystal was biased at –10 kV and was faced on both sides by two grounded silicon detectors (referred to as Si-in and Si-out). These detectors attracted and collected low-energy electrons emitted under ion impact by the entrance and exit surfaces. The signal they delivered had an amplitude proportional to the electron multiplicity.

A. Charge state, energy loss and electron multiplicity measurements

We have shown in a recent paper [14] that the electron multiplicity for channeled projectiles is smaller than for unchanneled projectiles or than in random conditions, because it reflects the reduction of the energy loss rate of channeled projectiles. Moreover the electron multiplicity has been shown to depend on the transverse energy of channeled projectiles. Hence, electron multiplicity can be used for discriminating between channeled projectiles of different transverse energies, and**,** of course, between channeled and unchanneled projectiles.

In fig 1, the position X of transmitted ions in the magnet focal plane is associated to the normalized electron multiplicity yielded by the detector Si-out, successively for a random orientation and for alignment along the (111) and (110) planar directions as well as along the <110> axial direction. This two-dimensional representation provides substantial information in addition to the simple spatial distributions at the focal plane. It must be noted that each picture results from the juxtaposition of spectra recorded for different values of the magnetic field of the spectrometer and that there is no dose normalization between adjacent spectra so that most of the rare charge states can be seen.

First, one sees that individual charge states may show up, except in the random orientation. In this orientation, transmitted ions are distributed rather uniformly in a large ellipse-shaped spot. The charge state distribution corresponds to charge equilibrium and is then gaussian-like. The mean charge is close to 74, in good agreement with the semi-empirical formula of Leon *et al.* [15]. In fact the charge state distribution at emergence reflects the one inside the target. As the ion energy loss has nearly a Q^2 dependence (for 20 MeV/u uranium ions at charge state equilibrium, the bound electrons are localized very near the nuclei and the ions are nearly point charges), the charge state fluctuations inside the target induces energy straggling. The very heavy ions at intermediate velocity used in our work experience very large charge-changing cross sections and, in this case, the energy straggling in random geometry is by far dominated by charge state fluctuations [16]. Of course, energy straggling smears out the position X distribution. However, even if not resolved, the X distribution reflects the charge state distribution: the higher the charge state, the stronger the deflection (hence X). We can notice that the electron emission yield, that reflects the energy loss rate of projectiles when they are about to leave the target, is seen to increase slowly with the charge state at emergence (from the arbitrary chosen value 1 to about 1.1), which is due to the fact that forward emitted electrons originate from a depth in the target that is not much larger than the mean free path for ion charge changing.

For (111) and (110) planar alignments, two components are clearly seen. The first one is random-like, however with a slightly higher mean value for the X distribution, and corresponds to the unchanneled part of the aligned beam (~34% and 42%, respectively). The second one is made of a succession of spots corresponding to individual charge states, from the best channeled projectiles of Q_{out}=91 at the extreme right to the poorly channeled projectiles of Q_{out}=70 at the extreme left. One may wonder why individual charge states can show up, especially for the lowest ones (70 to ~78) that are mixed up in random conditions and for the unchanneled component. As already indicated above, the mixing observed in these two latter cases is related to the strong energy straggling induced by charge changing events during the traversal of the target, electron capture, mainly by MEC and electron loss, mainly by NII. The emergent ions have reached charge equilibrium since long: according to the code ETACHA [2], this equilibrium is reached after 1 or 2 µm. On the contrary, for channeled projectiles the MEC probability is suppressed, or considerably reduced and the lower cross-section REC takes over. On the other hand electron loss by NII is suppressed and only the low cross section EII can occur. As a result the channeled component does not reach any charge equilibrium at emergence. The projectiles emerging in a given charge state have essentially captured electrons, and at about the same pace because they had nearly the same transverse energy and experienced nearly the same mean electron density. Then they suffered about the same mean energy loss. Moreover, as the charge exchange straggling is much weaker than that for ions in random conditions, the individual charge states can be clearly identified. We can take benefit from this feature to turn the position X scale into a Q_{out} scale, for ions emerging with a given energy, that can be used to obtain the Q_{out} distribution in random conditions.

For <110> axial alignment, the picture looks like what is observed in planar channeling except that the unchanneled component is too weak to be clearly visible. Note that, for the best channeled projectiles along both planar and axial directions, the individual spots do not appear vertical, but obliquely oriented. As the position X of a transmitted ion of a given charge state depends on its energy loss in the crystal, this shows that energy loss and forward electron emission are correlated, which is not surprising. This feature clearly shows up for the best channeled projectiles in the case of the <110> direction. In fig 2(a), the scatter plot of the highest charge states is shown, along with oblique lines that mark the separation

between charge states. In fig 2(b) we show the corresponding X distribution of the individual charge states, and also the X distribution of the direct incident U^{91+} beam. Then we can determine the mean energy loss of the frozen component of $Q_{out} = 91$, here 4.5% in units of the incident energy, which has to be compared to the tabulated mean energy loss in random conditions, 5.0 %. One learns more on energy loss in fig 2(c) where the two X distributions correspond to transmitted projectiles with electron multiplicities $N_{Si\text{-}out}$ respectively below 0.4 and above 0.9, and thus with, respectively, a relatively small or a large transverse energy. In particular, one can observe on fig 2(c) that for the frozen component, the energy loss ranges from 3.8% to more than 5.3%. This shows that the available area of the transverse space for the frozen component is rather large, and different frozen ions may experience different target electron densities, from a few 10^{-2} to a few 10^{-1} electron per $Å^3$ (the map of the electronic densities averaged along the silicon <110> axis has been calculated in the reference [17]). This explains why the $N_{Si\text{-}out}$ distribution corresponding to the frozen component is broad. Then, the frozen U^{91+} projectiles associated to high $N_{Si\text{-}out}$, may lose more energy than projectiles traversing the crystal in random conditions (with a mean charge state of 74). Of course, this is due to the quasi Q^2-dependence of the energy loss rate. However, even the frozen U^{91+} ions that suffer the highest energy loss rate are still well-channeled projectiles that experience reduced electron densities: their energy loss rate, when the charge dependence has been removed, is 0.7 times the random value. For the low $N_{Si\text{-}out}$ component, the non-monotonous decrease of the charge state fraction with decreasing charges is attributed to multiple electron capture events suffered by very well channeled projectiles in the thin amorphous surface layers on each side of the crystal. The simulations presented below have shown that the best agreement with experimental charge distributions is obtained for a total thickness of amorphous layers of 60 Å.

The experimental charge state distributions extracted from the results shown in fig 1 are given in fig 3: for a random orientation and for <110> axial alignment in fig 3(a), and for (111) and (110) planar alignments in fig 3(b). One of the main features we can notice in fig 3 is the mean charge state at emergence of poorly-channeled ions in axial and planar orientation;

In fig 3(a) we show also the results of Monte-Carlo simulations [18]. These simulations, that reproduce the general trends of the charge distributions, were based on the full description of ion trajectories and charge exchange in the crystal.

In fig 4 we show, for the <110> direction, how the measured charge fractions $F(Q_{out})$, for Q_{out} values from 91 to 86, vary with the angle ψ_0 between the incident beam direction and the <110> direction. These charge states, that disappear when ψ_0 increases (because they do not show up in random conditions), represent the best channeled part of the aligned beam Note that trying to reproduce these variations is a very severe test for the simulations that we have performed (see section III).

B. X-ray measurements

X-ray measurements provide additional information on the nature and probabilities of the charge exchange processes [19]. The Ge detector we used allowed us to observe the filling of the K- and L-shells of the H-like incident ions. In fig 5 we show two X-ray spectra obtained with a tightly collimated detector located at 90° to the beam direction, for a random incidence (fig 5(a)) and for alignment along the <110> axial direction (fig 5(b)). These spectra are normalized to the same number of non frozen ions. This normalization is based on the fact that the filling of the K-shell vacancy occurs at most once (excitation or ionization from the K-shell of uranium ions can be neglected).

The spectrum of fig 5(a) is dominated by L- and K- photons that are mainly due to decay cascades following MEC events. For 20 MeV/u uranium projectiles in a silicon target, these cascades are due essentially to the capture of silicon K-shell electrons into ($n \geq 4$) shells of uranium ions (this is required by the necessary matching of the initial and final velocities of the captured electron). Moreover the REC lines are essentially absent because the K- and L-REC cross sections are smaller than MEC cross sections by orders of magnitude. K- and L-shells are very rapidly filled by the cascading processes following MEC events and thus K- and L-REC events cannot occur. In contrast, in the spectrum of fig 5(b), the L-lines are strongly reduced and L- and K-REC lines do show up because the MEC probability is drastically reduced for channeled projectiles. K-lines still appear. They originate from the radiative decay following capture events either by MEC, into high *n*-shells, or by REC, mainly on the L-shell. On the other hand, the sharp components of the L-lines observed in fig.5(a), which correspond to cascade events taking place after charge state equilibrium has been reached (*i.e.* cascade between rather well defined energy levels), has disappeared in the spectrum obtained in the <110> orientation (fig.5(b)). The main reason of this effect is obvious: most of the ions are well channeled, they experience reduced capture probabilities and exit the crystal with few electrons on their L-shell. However the effect also concerns less well channeled ions that do experience significant electron capture. For instance, ions with "intermediate" transverse energies may approach atomic strings close enough to experience many MEC events, filling progressively their L-shell. However they are too far to undergo ionization in this shell, as such an event requires atomic collisions at very small impact parameters of the order of 10^{-2} Å. Finally we have shown in ref.[18] that even the ions with very high transverse energy, do not show up the sharp components of the L-lines. As these ions approach enough atomic strings to suffer L-shell ionization, this result proves that the filling of the L-shell takes place much less rapidly than for unchanneled ions. We have attributed this fact to a so-called "superdensity effect": a capture in an excited state is often followed by re-ionization before that the captured electron could be stabilized in an inner shell.

For <110> alignment, we show in fig 6 the dependence on Q_{out} of the various REC and MEC rates, for Q_{out} values ranging from $Q_{out} = 90$ (that correspond to the best channeled projectiles producing X-rays), to $Q_{out} = 76$ (that correspond to rather poorly channeled projectiles). These rates have been determined by assuming that radiative decay emission is isotropic in the projectile frame, and that REC photons are emitted according to a $\sin^2\theta$ law [20, 21], where θ is the angle between the photon and the beam directions in the laboratory frame. In fig 6(a) we give the Q_{out} dependences of K-REC, L-REC and L-line (Balmer) photon rates per ion transmitted with the charge Q_{out}. The decrease of the Balmer rate when Q_{out} increases is due to the progressive suppression of MEC events when the transverse energy decreases. Then, as already stated, the K- and L-shells vacancies of ions with low transverse energy are not filled by MEC and these projectiles may experience large radiative capture rates. In fig 6(b) we give the relative contributions of REC and MEC processes to electron capture. The main feature of this figure is that mechanical capture is the dominant process as soon as ions capture more than one electron whereas its contribution for ions transmitted with the charge state $Q_{out} = 90$ is about 30%. This is a qualitative evidence for a rapid increase of the MEC probability with the ion transverse energy, i.e. when projectiles can approach closer to atomic strings or planes.

The experimental results presented in fig 4 and fig 6 provide very detailed information on the rate of the various electron capture processes as a function of the ions transverse energy. This information could be reached because we used very heavy H-like ions at intermediate velocities (beams extracted after deceleration from the storage ring at GSI).

Then: i) the charge state at emergence is strongly connected to the transverse energy. ii) the very high electron capture probability allowed us to accumulate sufficiently high statistics X-ray spectra to perform a detailed analysis of these spectra for each charge state Q_{out} at emergence.

The transverse energy of an ion defines its available transverse space, and thus its impact parameter distribution with respect to target nuclei. We have then attempted to fit our experimental results in order to reach information on the competition between REC and MEC events as a function of the impact parameter, and thus on the impact parameter dependence of the MEC probability per target atom. For this purpose, we have performed simulations that are presented in the next section.

III. Simulations

Simulations are necessary to get quantitative information out of our experiments. We show in what follows that for simulating the charge exchange of rather well channeled projectiles, that keep far from atomic strings or planes, typically at distances larger than 0.25 Å, a full Monte Carlo calculation is not mandatory. We have used a much less time consuming approach, based on the following strategy: first, impact parameter distributions are determined by trajectory calculations, neglecting charge exchange. Second, electron capture rates are adjusted as a function of the ion transverse energy in order to reproduce the experimental data. Third, we extract the impact parameter dependence of MEC and REC capture per target atom by unfolding the preceding values..

A. Impact parameter distribution as a function of transverse energy

Simulating charge exchange events requires essentially to determine the impact parameter distribution of channeled projectiles and the mean electron density they encounter. We have therefore performed calculations of channeled ion trajectories all along the crystal For each crystal orientation (axial and planar), this procedure allowed us to set the impact parameter distribution and the mean electron density encountered as a function of the transverse energy.

Impact parameter distributions were calculated considering the successive collisions suffered by projectiles. For this, we used the Moliere analytical approximation of the Thomas-Fermi screening function to calculate the ion-atom potential. The distribution of thermal displacements of target atoms from lattice sites was considered to follow a gaussian law with a variance calculated from the Debye theory. Correlation between atomic displacements was neglected. Then we used the transverse continuum potential approximation to provide the transverse energy value $E_\perp$ (this approximation was not used for trajectory calculations)**.**

The transverse energy distribution at the crystal entrance is somewhat modified along the ion path. This is due, on the one hand, to transverse energy changes related to charge exchange and, on the other hand, to multiple scattering. Let us first evaluate the influence of charge exchange, which has been studied in detail by Grüner *et al.* [22]. The variation $(\Delta\varepsilon_\perp)_{\Delta Q}$ of the reduced transverse energy $\varepsilon_\perp = \frac{E_\perp}{Q}$ of a channeled projectile due to a charge change ΔQ occurring when its trajectory makes the angle ψ with the channeling direction is $(\Delta\varepsilon_\perp)_{\Delta Q} = -(\Delta Q)E\psi^2/Q^2$. As the dominant charge exchange (the mechanical capture) occurs mainly at the closest approach of the atomic strings or planes, *i.e.* when ψ has the smallest

values, $(\Delta\varepsilon_\perp)_{\Delta Q}$ is small compared to $-(\Delta Q)E\psi_c^2/Q^2$ (where ψ_c is the Lindhard critical angle) that is of the order of 1 eV for ΔQ=1 in the <110> direction. As the potential heights along the axial and planar directions we have studied are respectively about 120 eV and 20 eV, the influence of charge changing on the channeled projectile trajectories has been neglected in our simulations.

As for transverse energy changes induced by multiple scattering, the effect of elastic collisions is already taken into account in the trajectories calculations that are achieved by considering all the consecutive binary collisions with target atoms. But multiple scattering on target electrons must also be considered; it is in fact the main source of transverse energy change for well channeled ions. According to Bonderup *et al.* [23], one may neglect the contribution to multiple scattering of non local distant interactions and the mean rate of transverse energy increase induced by this process is connected to the energy transfer by close collisions on target electrons. Thus we calculated the mean increase of the transverse energy using the measured energy loss values and considering only the fraction of this loss that can be attributed to close collisions (this procedure is described in ref [10]). The increase in transverse energy is small but not negligible and was considered in the simulations.

There is a one-to-one relationship between the transverse energy of an ion and its minimum distance of approach to atomic strings or planes r_{min}. In the following paragraph, we will mostly consider r_{min} distributions. They give access to the impact parameter distribution with respect to target atoms, which has to be determined in order to extract information on the impact parameter dependence of charge exchange processes from our experimental data.

B. Charge exchange

For poorly channeled ions, the charge state at emergence arises from a competition between capture by MEC and ionization by NII, both types of events occurring very frequently. For these ions the r_{min} distribution varies strongly with the penetration depth. In such a situation the information that can be reached from our experiments on the impact parameter dependence of MEC probability would be questionable at small impact parameters. We will thus focus on electron capture events of channeled ions that remain at distances r_{min} larger than about 0.25 Å from atomic strings or planes. At such distances, the projectile ionization by nuclear impact (NII) is strongly reduced and was neglected in our simulations (this approximation is justified in section IV B). The projectile electron loss can therefore occur only by EII of electrons captured in outer shells (that had not enough time to cascade into inner shells). In order to limit the number of parameters in our simulations, we have introduced an effective capture probability defined as the probability of capturing an electron that is not lost afterwards (of course, this probability results both from capture events and from electron loss through EII).

Our simulations of charge exchange are based on the determination of the minimum distance $r_{\min}^i$ distributions near the entrance crystal surface. These distributions depend on the beam angular divergence and on the crystal orientation. We consider their evolution induced by electron multiple scattering, as a function of penetration depth. To each $r_{\min}^i$ value, we associate the mean numbers of effective mechanical and radiative capture events, N_{MEC} and N_{REC}, and a mean transverse energy increase per unit path, $\overline{d\varepsilon_\perp}/dz$, proportional to the mean energy loss per unit path $\overline{dE}/dz$ [23]. The $\varepsilon_\perp$ increase results in an increase with depth of the transverse accessible space, *i.e.* a r_{min} decrease and a capture probability increase.

The influence of the projectile charge state on the capture probabilities is taken into account: whereas the mechanical capture does not depend much on the projectile charge state (since it

occurs in highly excited states), the REC probability for an U^{90+} ion (that has no K-vacancy) is for example 30 % lower than for a H-like U^{91+} ion. The electron capture events occurring in the amorphous layers of the crystal surfaces are also taken into account in the simulations.

The adjustable parameters introduced in the simulations are the following: i) the mean numbers $N_{MEC}\left(r_{\min}^{i}\right)$ of mechanical capture events for each of <110>, (110) and (111) directions; ii) a coefficient C_{REC} (this coefficient is justified below) applied to the REC cross section (this cross-section is readily obtained in the frame of the non-relativistic dipole approximation [21]); iii) the beam angular divergence (that could not be measured separately); iv) the electron capture in the amorphous layers. The main experimental data that have been used to constrain these parameters are (see section I): the charge state distributions, the K-, L-REC probabilities and the angular scans of the emergent charge state distribution across the <110> axis (and across the (110) and (111) planes, which were also obtained even if not presented here). In order to fit these scans, we had to assume a two-component beam profile: 65 % of the beam described by a narrow gaussian distribution with 1D standard deviations $\sigma_X=\sigma_Y=0.14$ mrad and the remaining 35 % by wider Gaussian wings with $\sigma_X=\sigma_Y=0.43$ mrad, to be compared to the critical angle of 1.4 mrad for the <110> axis, and of 0.50 and 0.55 mrad respectively for the (110) and (111) planes.

The overall best agreement between the simulations and the measurements, presented in fig. 4, 6.b and 7.b, leads to the mean effective capture numbers $N_{MEC}\left(r_{\min}^{i}\right)$ and $N_{REC}\left(r_{\min}^{i}\right)$ given in fig. 7.a. In all cases, the agreement between the numerous experimental data and the simulations is remarkable. In figure 7.b we compare the simulated and measured charge state distributions for the <110>, (110) and (111) orientations. Having limited our simulations to ions of relatively low transverse energy, that undergo less than nine effective captures, the ions that capture more than ten electrons are gathered in the fraction called F(Q_{out}<82). The mean effective captures N_{MEC} presented in fig 7.a for $r_{\min}^{i}$ > 0.25 Å correspond to the simulations providing the best overall agreement with the data. N_{MEC} increases strongly for ions that approach the atomic strings or planes at distances $r_{\min}^{i}$ smaller than about 0.4 Å, a distance that roughly corresponds to the spatial extension of the silicon core orbitals. On the contrary, the mean number N_{REC} is nearly constant although the mean density $\overline{\rho_e}$ ($r_{\min}^{i}$ =0.3 Å) is about twice the mean density $\overline{\rho_e}$ ($r_{\min}^{i}$ =0.8 Å) sampled by well channeled ions. This is due, for poorly channeled ions of small $r_{\min}^{i}$ values, to the fast filling (close to the crystal entrance) of their inner shells by MEC followed by electron cascades.

C. Impact parameter dependence of MEC probabilities

Our experimental results and the above simulations provide the effective MEC probability $P_{MEC}^{eff}(b)$ per target atom at a given impact parameter *b*. This probability is deduced from the mean numbers $N_{MEC}\left(r_{\min}^{i}\right)$ of MEC events and from the impact parameter distributions $\Phi_{r_{\min}^{i}}(b)$ by assuming independent single charge exchange events for well channeled ions. $N_{MEC}\left(r_{\min}^{i}\right)$ and $\Phi_{r_{\min}^{i}}(b)$ are then linked, for a given crystal direction, by the following relation:

$$N_{MEC}\left(r_{\min}^{i}\right)=\int P_{MEC}^{eff}(b)\Phi_{r_{\min}^{i}}(b)db\,. \qquad (1)$$

Within the experimental uncertainties, the probability $P_{MEC}^{eff}(b)$ is found to be the same for the three crystal directions studied (<110>, (110) and (111)), a strong indication of the

self-consistency of our simulations. The larger $N_{MEC}\left(r_{\min}^{i}\right)$ values obtained for the (110) plane (see the fig 7.a) is explained by the fact that the impact parameter distribution $\Phi_{r_{\min}^{i}}(b)$ in this plane is slightly shifted towards the small impact parameters compared to the impact parameter distributions obtained for the <110> and (111) directions.

IV. Discussion and comparison with theoretical calculations

A. REC cross sections

Detailed information on the radiative capture (namely the influence of the electron gas polarization) has been reported and discussed already in [24]. In this paper, we observed that theoretical REC cross sections have to be multiplied by a factor C_{REC}=1.5 to reproduce our results. This is explained by a ion-induced polarization of the target electron gas resulting in a local electron density enhancement in the vicinity of these slow, highly charged projectiles. In order to complement this point, we present in fig 8 the measured evolution of K-REC cross sections as a function of the adiabaticity parameter. The gas and amorphous solid target data correspond to a compilation by Th. Stöhlker *et al.* [25]. Channeling data were obtained by our collaboration at GANIL [26, 27] and in the present work. The theoretical values correspond to the calculations of ref. [21] performed in the frame of the non-relativistic dipole approximation and they correspond to non-perturbed electron densities in the target. At low energies, measurements on solid state targets tend to exhibit enhanced cross sections when compared either to measurements on gas targets or to theoretical estimates. In contrast, at higher energies, *i-e* in situations for which $\eta>1$, a good overall agreement is observed.

These results for REC cross sections suggest some remarks: as discussed in ref. [24], a very strong electron gas polarization is induced by the relatively slow and very highly charged ions used in the present experiment. In such a situation, first order perturbation calculations predict a very strong enhancement of the electron density at the ion site that should induce an enhancement of the REC yield much higher than the 50% effect that we observe experimentally. In fact, higher order–or non-perturbative - calculations would be required to get a quantitative estimate of the density enhancement. Besides, although channeling conditions are the most efficient way to measure REC cross sections in solids at such low values of the adiabaticity parameter, gas target measurements would certainly provide complementary information on the observed electron density enhancement observed in channeling conditions and on the validity of the dipole approximation at low η values.

B. Effective MEC probabilities per target atom

In fig 9, we show the *b* dependence of the probability $P_{MEC}^{eff}(b)$ extracted from our experimental results, *via* eq.1, along with CDW-EIS calculated values of MEC probabilities $P_{MEC}^{theory-n}(b)$. The error bars become important for *b* values smaller than 0.2 Å, because the assumptions subtending our treatment are only valid for relatively well-channeled ions; they also become important for *b* values above 0.55 Å because, at large *b* values, the electron capture events are rare and mainly due to REC.

The CDW-EIS calculations were limited to capture into shells with *n*-value ≤ 5 because of the enormous complexity of such analytical methods. The sum of these theoretical probabilities is larger than the probability $P_{MEC}^{eff}(b)$ for impact parameters *b* below 0.15 Å. This could be expected as, for small *b* values, NII becomes important and thus $P_{MEC}^{eff}(b)$ is strongly affected by electron loss events. On the contrary, this sum is much smaller than

$P_{MEC}^{eff}(b)$ at large impact parameter. This confirms the dependence on the shell number, *n*, of the integrated CDW cross sections [28] presented in fig 10: the mechanical capture probability is maximum for final states *n* equal to 5 and 6 (which are not considered in the CDW-EIS calculations) and then decreases for larger *n*-shells. The decrease predicted by ref [28] and presented in fig 10 is much slower than the n^{-3} scaling law usually assumed [29]. Indeed, the mechanical capture requires the overlap of the initial and final wave functions of the captured electron, which leads, in our experimental situation, to a high probability of electron capture from the silicon K-shell into the projectile outer shells. Besides, since the silicon K-shell extension is very small (of the order of 0.05 Å), the MEC probability is expected to depend mainly on the projectile orbitals on which a K-shell target electron is captured; this has been verified by comparing $bP_{MEC}^{theory-n}(b)$ functions up to *n*=5 and $b|\varphi_n(b)|^2$ (where $\varphi_n(b)$ is the radial wave function of the H-like uranium). These two functions appear to be nearly similar and we used this similarity to extrapolate the theoretical probability $P_{MEC}^{theory-n}(b)$ for *n*>5. The overall electron capture probabilities on all the projectile shells (indexed by *n*) and the corresponding sum for *n*-values running from *n* =1 to *n*=10 are presented on fig 9**.** The fact that these theoretical probabilities are much larger than the probability $P_{MEC}^{eff}(b)$ of effective capture for impact parameters *b* above 0.25 Å demonstrates the importance of EII on outer shells (let us recall that the values $P_{MEC}^{eff}(b)$ that were obtained when fitting our experimental data by simulations result from both capture and ionization processes).

In order to really compare the experimental and theoretical results for impact parameters *b* > 0.25 Å, we have evaluated the projectile ionization probability to deduce a theoretical probability for effective capture $P_{MEC}^{theory-eff}(b)$. The nuclear impact ionization (NII) is negligible for impact parameters *b* > 0.25 Å: the outer shell electrons of the projectile with *n*-value close to 6 or 7 present binding energies of the order of a few keV and orbital extensions of about 0.2 Å. As the ionization of these electrons requires impact parameter smaller than 0.05 Å between projectile electrons and silicon atoms, the NII process is much less important than the EII process for impact parameters *b* above 0.25 Å. The EII probability has been estimated by coupling the cross sections $\sigma_{EII}(n)$ for electron impact ionization of the projectile *n*-shell to the radiative decay times and to the decay branching ratios that correspond to the probability for an electron initially on a *n*-shell to reach a *n'*-shell with *n'*<*n*. The cross sections $\sigma_{EII}(n)$ have been deduced from the cross section $\sigma_{EII}(n=3)$ determined for 29 MeV/u Pb^{56+} ions by L'Hoir *et al.* [18] and a scaling law based on the Lotz formula [30]. The radiative decay time and the branching ratio have been obtained from the calculations of Omidvar for H-like ions (with a Z_p^{-4} scaling law for the decay times) [31]. The EII process leads to a complete ionization of the shells above *n*= 9 whereas it does not much affect the probability for electron capture on the other shells.

The theoretical probability $P_{MEC}^{theory-eff}(b)$ for effective capture is compared, in fig 11**,** to the probability $P_{MEC}^{eff}(b)$ deduced from our measurements. These two probabilities are in good agreement. This is a good indication that: i) the CDW-EIS calculations provide a realistic impact parameter dependence for MEC at medium and large distance; ii) our extrapolated estimates of MEC probabilities on high *n>5* shells (total cross sections, impact parameter dependence) are valid and thus MEC into highly excited states plays a major role. We are currently undertaking CTMC calculations to provide complementary estimates of the capture probability and confirm our extrapolation procedure.

Conclusion

Whereas full Monte Carlo calculations are required to follow the evolution of charge states and electronic configuration of high transverse energy channeled ions approaching atomic strings [14], we have shown that one may use a simpler calculation procedure based on the ion flux distributions when only relatively larger distances from target atoms are considered. This has allowed us to determine the dependence of MEC and REC probabilities by fast heavy ions as a function of impact parameters. REC probabilities are increased by the local electron density enhancement induced by the very heavy and highly-charged ions at intermediate velocities. Experimental MEC probabilities are consistent with the results of CDW-EIS calculations performed up to n=5 and extrapolated for larger n-shells. Our experiments have shown that the mechanical capture at large impact parameter arises mainly from capture into highly excited states, up to n=9. Besides, we have seen that frozen U^{91+} projectiles channeled in a 11.7 µm crystal may lose more energy than projectiles traversing the crystal in random conditions. This charge state effect has been used in a recent experiment to study the feasibility of strongly slowing down very highly charged ions by transmission through a relatively thick crystal in channeling conditions. The capture cross sections of the best channeled ions is so strongly reduced that they may have a significant probability to emerge with their initial charge state. The results of this study are to be published in a forthcoming paper.

In view of the future FAIR accelerator in Darmstadt, our work stresses the interest of channeling for the study of recombination and energy loss of the slow, highly-charged ions that will be available at the FLAIR facility.

Acknowledgments

This work was partly supported by the French-German GSI-IN2P3 collaboration agreement 97-35.

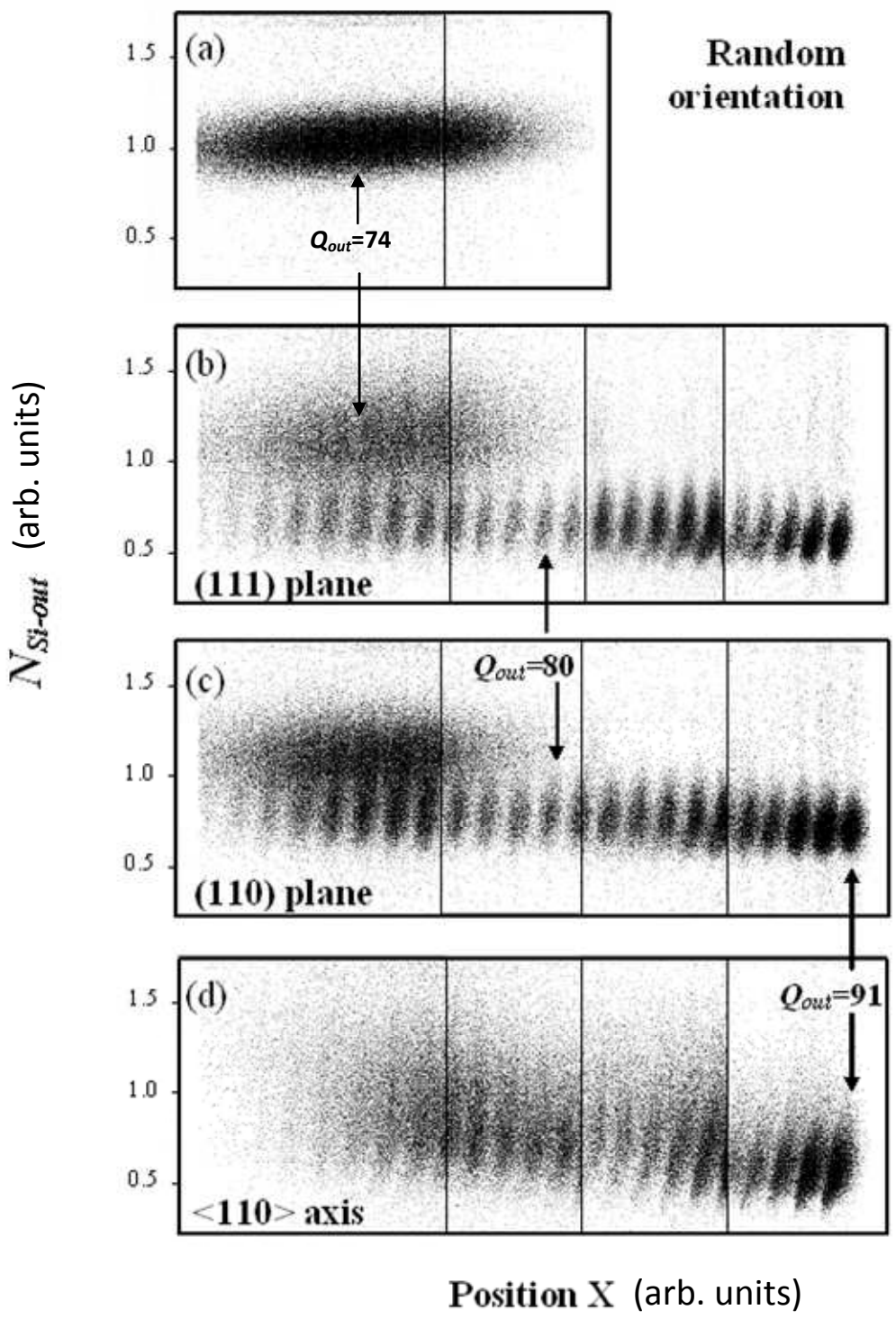

fig 1. Detection of projectiles transmitted for various beam incidence conditions of U^{91+} ions: (a) random incidence, (b-c) (111) and (110) planar alignments, (d) <110> axial alignment. Scatter plots of forward electron emission multiplicities ($N_{Si\text{-}out}$) as a function of X, the position in the focal plane of the analyzing magnet. $N_{Si\text{-}out}$ values have been normalized in such a way that the mean value of the left part of plot (a) is equal to unity.

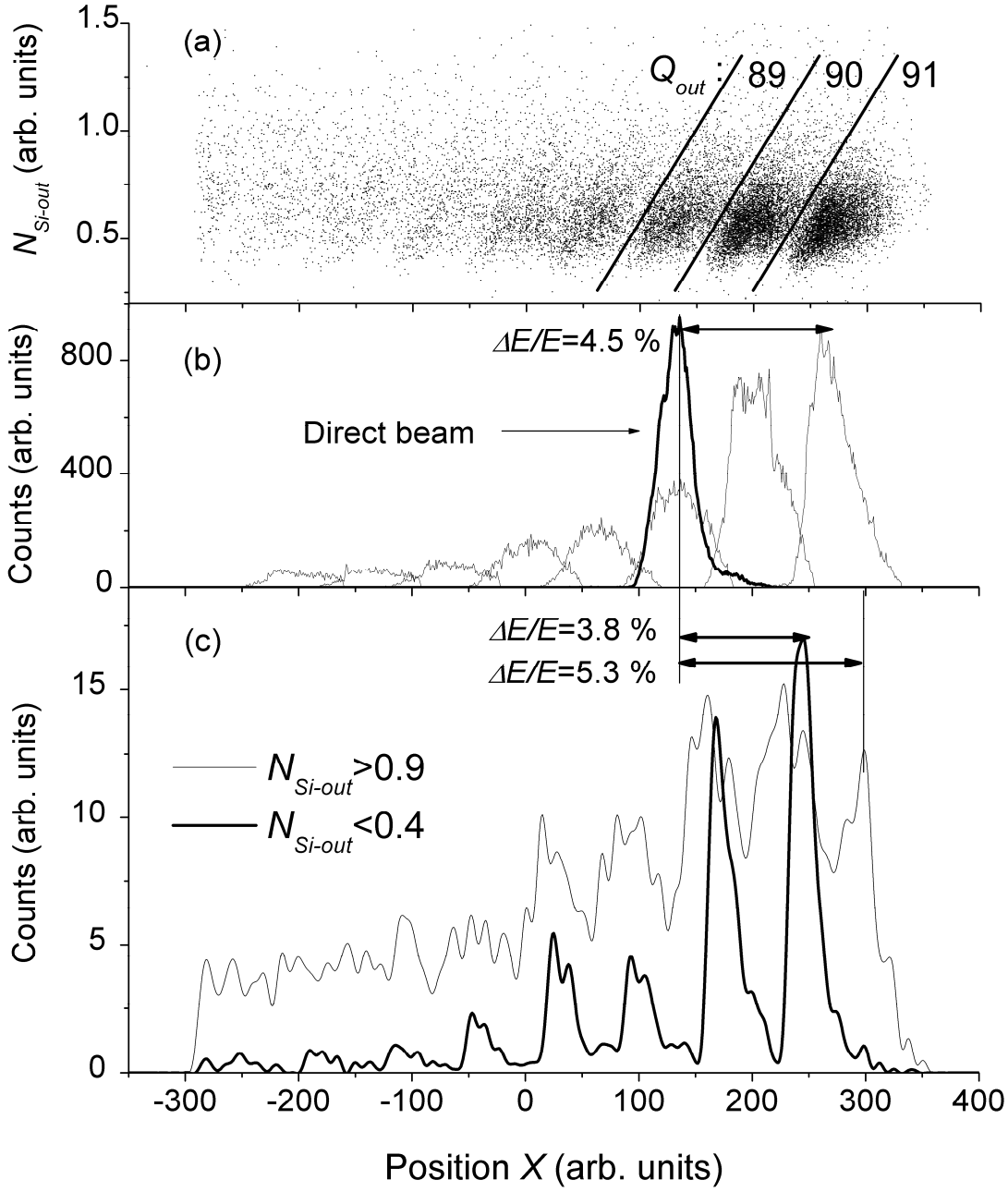

fig 2. (a) Scatter plot of forward electron emission multiplicities *vs* position X for the best channeled projectiles incident along the <110> axial direction. The oblique lines are used to delimit charge states and (b) generate, by projection, the X distribution of each charge state; the X distribution of the direct 91+ incident beam is also shown, which yields the energy loss of the frozen fraction.(c) Here two X distributions are shown, for transmitted ions of $N_{Si\text{-}out}$ above 0.9 and below 0.4, respectively (these distributions have been smoothed).

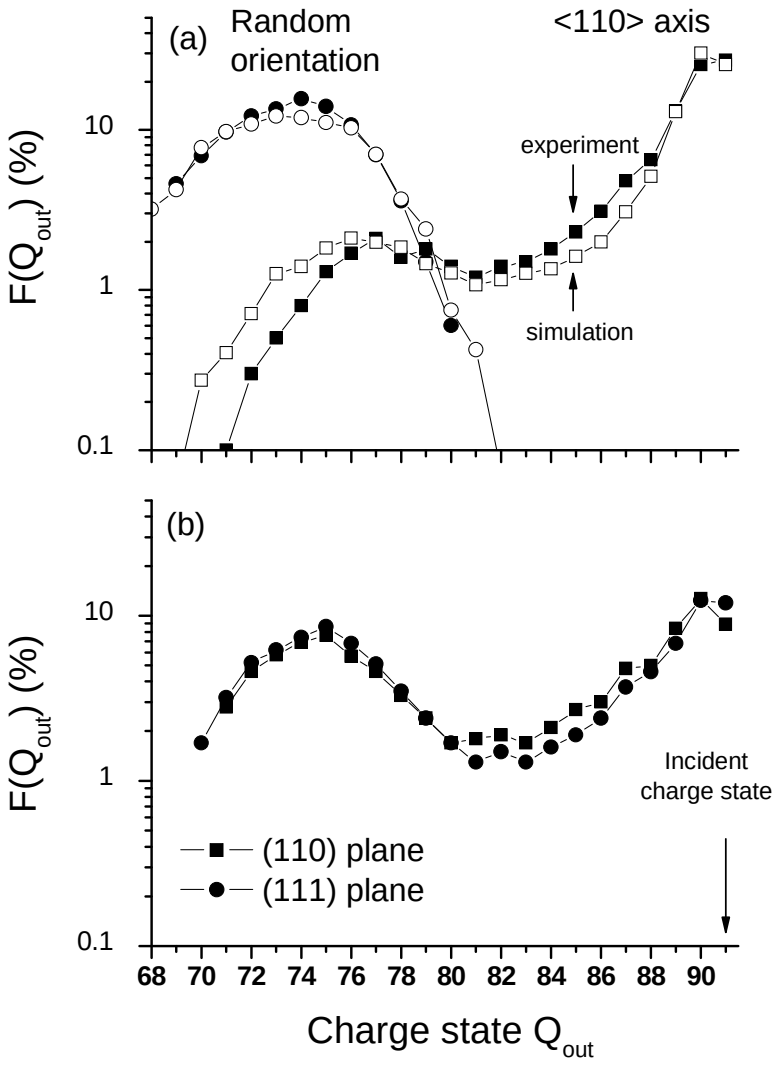

fig 3. Experimental charge distributions, $F(Q_{out})$, of incident 20 MeV/u U^{91+} ions transmitted (a) in random conditions and for <110> axial alignment (along with Monte-Carlo simulations). Full symbols: experiment, open symbols: simulations by L'Hoir *et al.* (see text); (b) for (111) and (110) planar alignments.

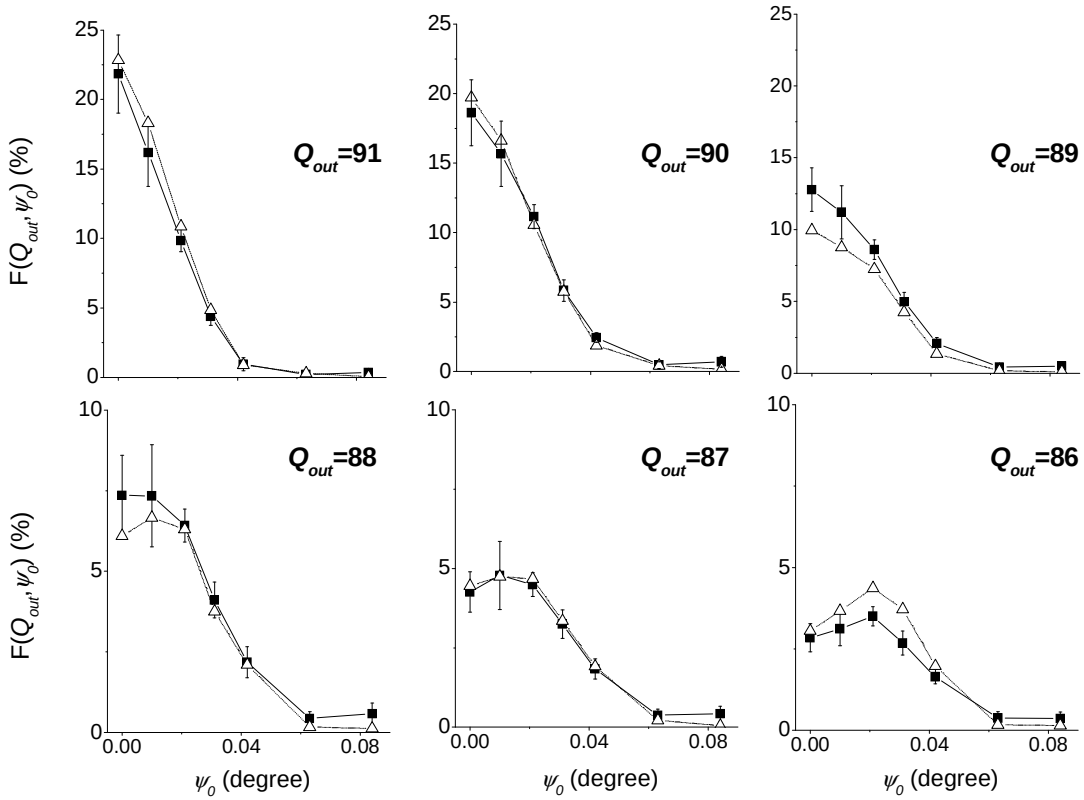

fig 4. Experimental (■) and calculated (△) variations with the angle ψ_0 between the incident beam direction and the <110> axial direction of the charge fractions, $F(Q_{out})$, for Q_{out} values from 86 to 91.

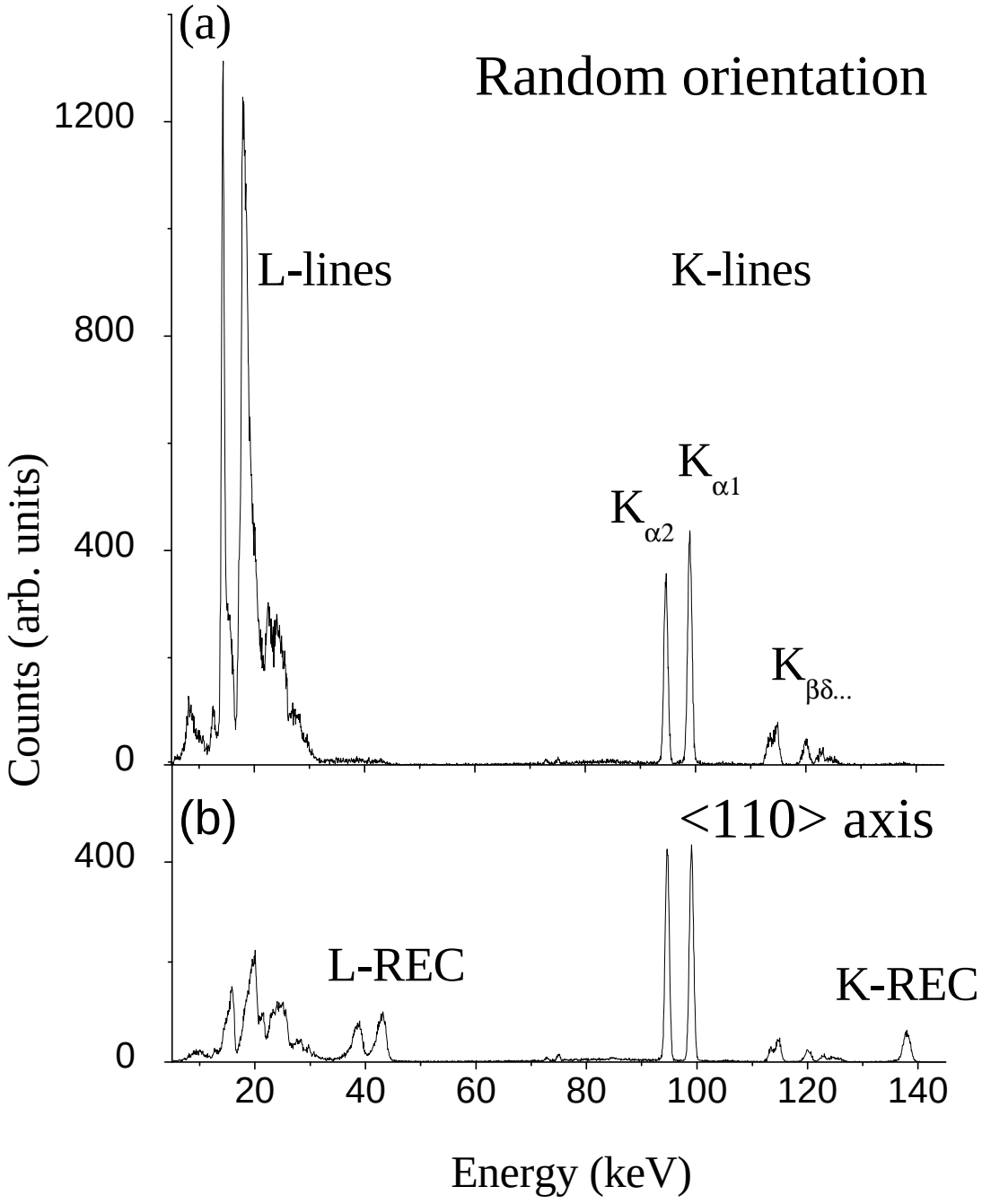

fig 5. Spectra of X-rays detected by a Ge detector located at 90° to the beam direction for a random incidence (a), and for incidence along the <110> axial direction. The spectra correspond to the same number of non frozen transmitted ions.

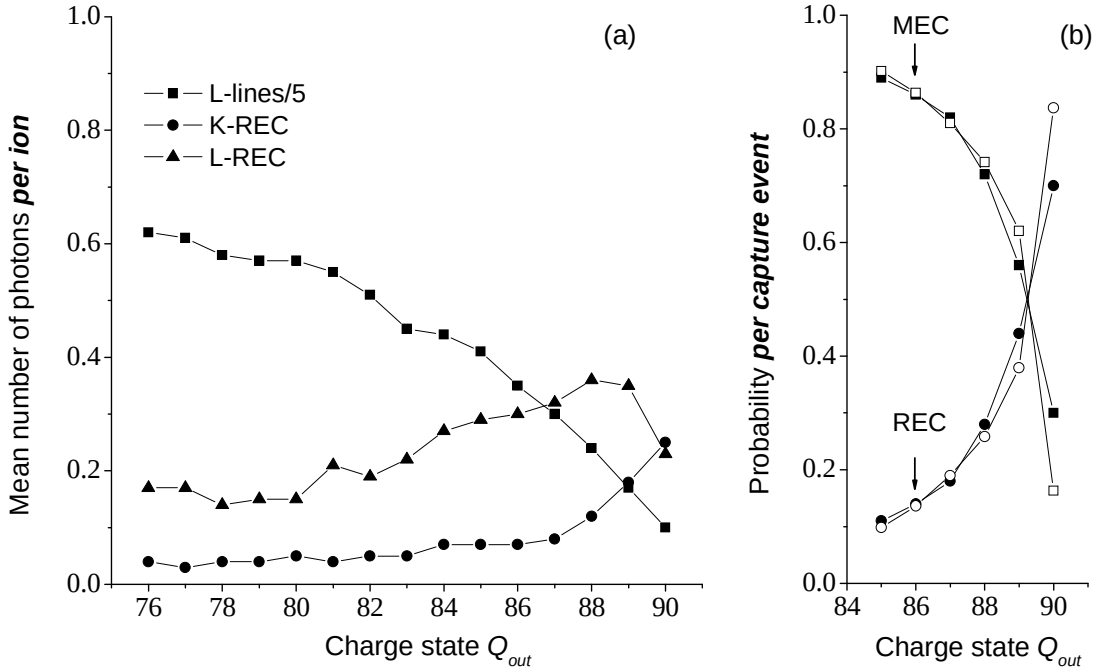

fig 6. <110> alignment: experimental Q_{out} dependences (a) of the rates per ion transmitted with the charge Q_{out}, of K-REC, L-REC and Balmer events, (b) of the relative contributions of REC and MEC to electron capture (full symbols) along with the simulation results (open symbols).

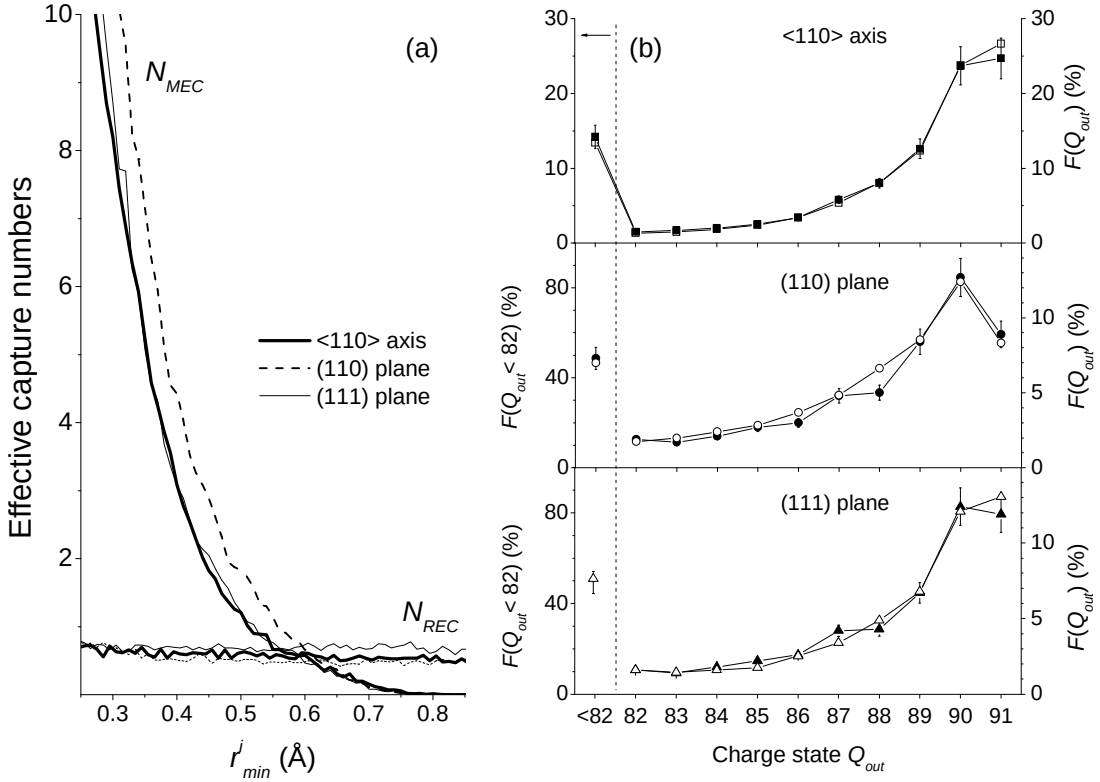

fig 7. (a) Simulated distributions of the mean effective mechanical and radiative capture numbers N_{MEC} and N_{REC} as a function of the minimal distance $r^i_{\min}$ of approach to the atomic strings or planes at the crystal entrance. (b) measured (full symbols) and simulated (open symbols) charge state distributions $F(Q_{out})$ for U^{91+} incident ions channeled along the <110> axis and the (110), (111) planes of the 11.7 µm silicon crystal.

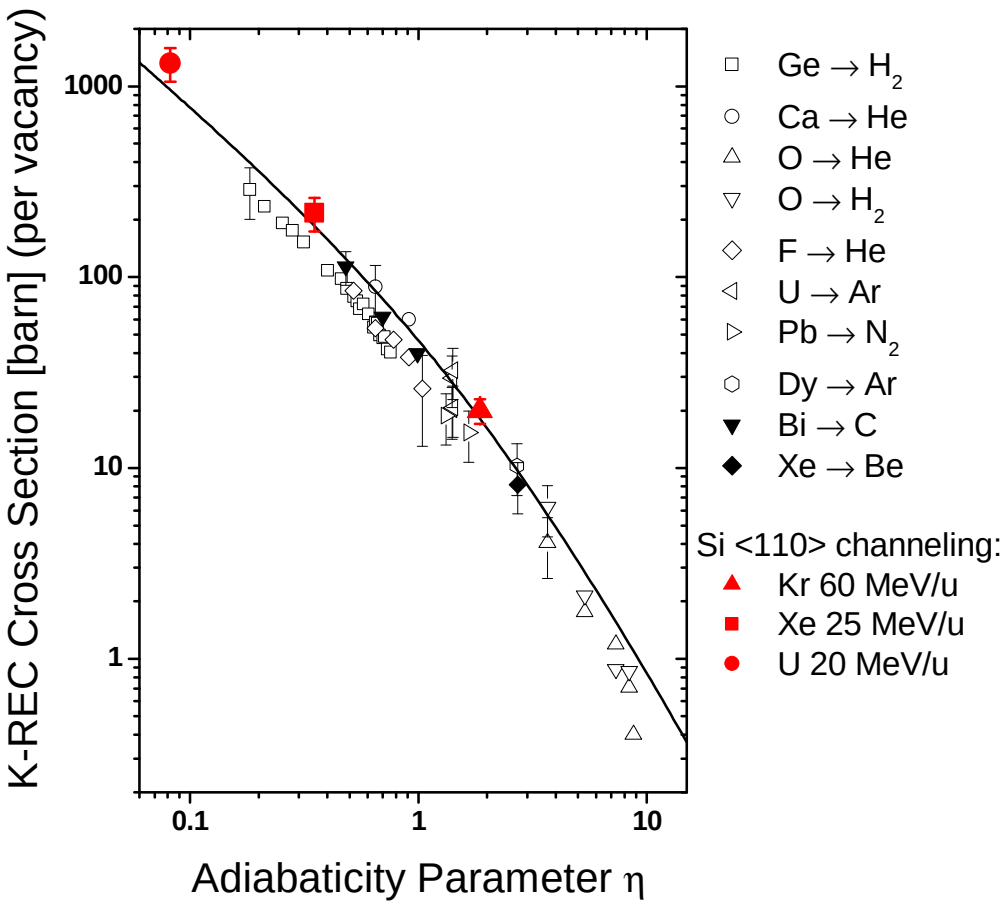

fig 8. K-REC cross sections (per K-vacancy) per target electron, as a function of the adiabaticity parameter. Hollow symbols: gas target data. Filled symbols: solid target data. Gas and amorphous solid data are taken from ref. [25]. Si<110> channeling data are from ref. [26] for Kr ions, ref. [27] for Xe ions, and present work for U ions. The solid curve corresponds to the non-relativistic dipole approximation [21].

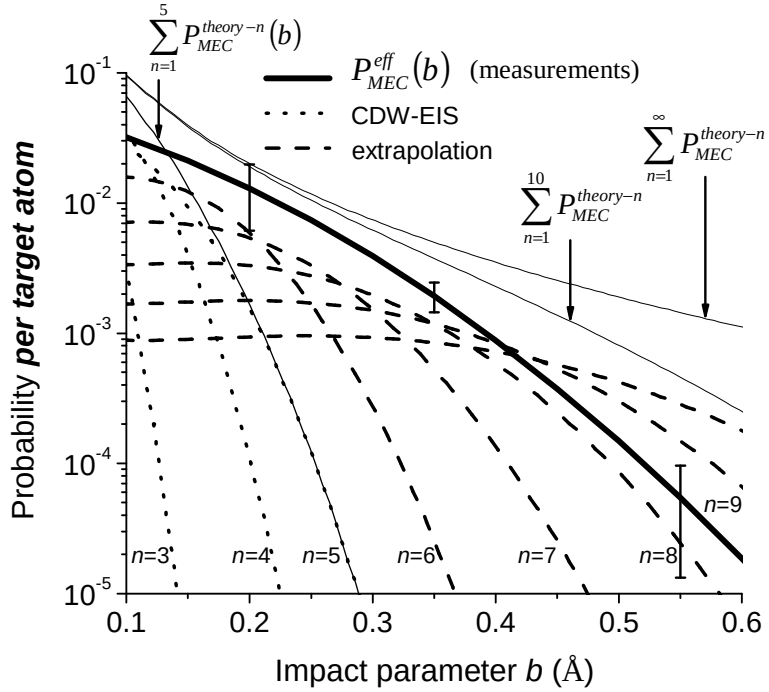

fig 9. Probability $P_{MEC}^{eff}(b)$ of effective MEC per target atom: our measurements (through simulations) (bold solid line), theoretical probability $P_{MEC}^{theory-n}(b)$: CDW-EIS probabilities of mechanical capture up to *n*=5 (dotted lines), extrapolated for larger *n*-values (dashed lines).

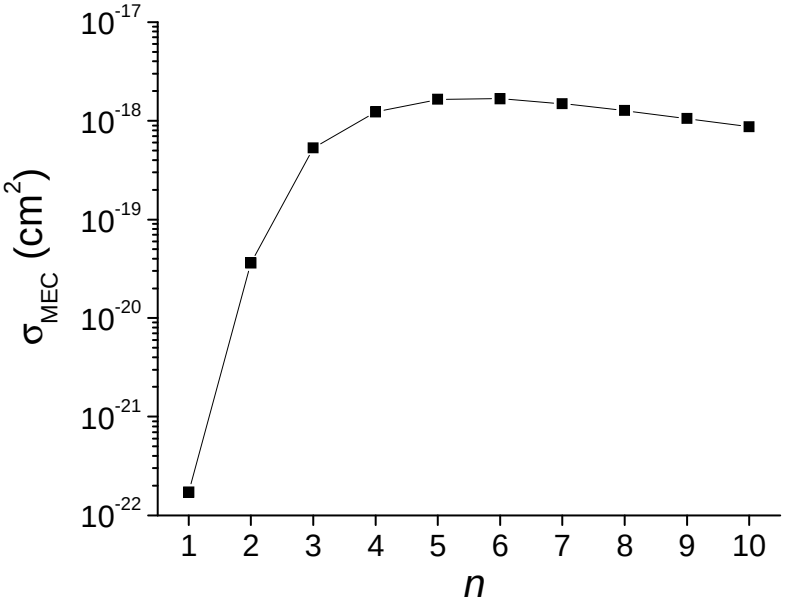

fig 10. Partial MEC cross sections for 20 MeV/u U^{91+} ions in silicon as a function of the final *n*-state (CDW calculations [28])

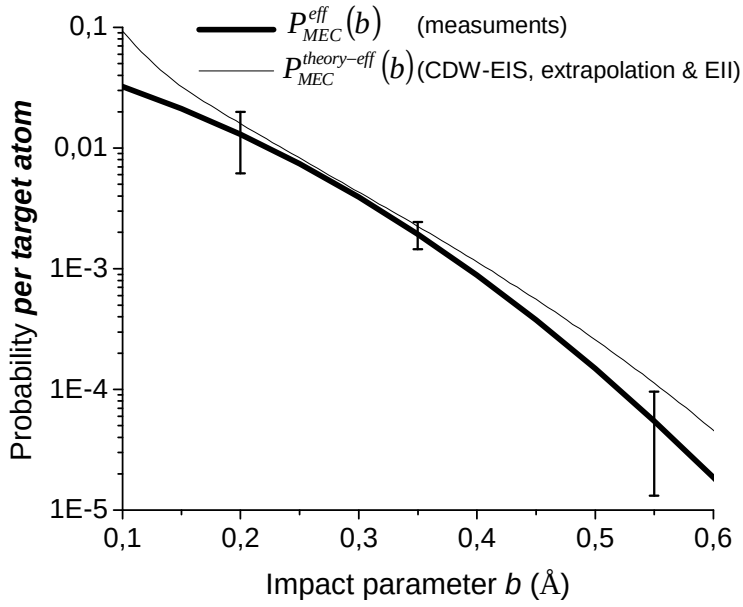

fig 11. Probability $P_{MEC}^{eff}(b)$ of effective MEC per target atom deduced from our measurements (through simulations) (bold solid line) and the theoretical probability $P_{MEC}^{theory-n}(b)$ (solid line) that is the sum of the CDW-EIS probabilities for mechanical capture on all projectile shells after modification for taking the electron impact ionization (EII) into account.

References

[1] F. Hubert, R. Bimbot, and H. Gauvin, At. Data and Nucl. Data Tables **46**, 1 (1990).

[2] J. P. Rozet, C. Stéphan, and D. Vernhet, Nucl. Instr. and Meth. B **107**, 67 (1996).

[3] R. Moshammer, P. D. Fainstein, M. Schulz, W. Schmitt, H. Kollmus, R. Mann, S. Hagmann, and J. Ullrich, Phys. Rev. Lett. **83**, 4721 (1999).

[4] J. Ullrich, R. Moshammer, R. Dörner, O. Jagutzki, V. Mergel, H. Schmidt-Böcking, and L. Spielberger, J. Phys. B **30**, 2917 (1997).

[5] K. L. Wong, W. Wu, E. C. Montenegro, I. Ben-Itzhak, C. L. Cocke, J. P. Giese, and P. Richard, J. Phys. B **29**, L209 (1996).

[6] J. Lindhard, Dan. Mat. Fys. Medd. **34**, 14 (1965).

[7] S. Datz, C. D. Moak, T. S. Noggle, B. R. Appleton, and H. O. Lutz, Phys. Rev. A **179**, 315 (1969).

[8] C. Cohen and D. Dauvergne, Nucl. Instr. and Meth. B **225**, 40 (2004).

[9] D. S. Gemmell, Rev. Mod. Phys. **46**, 129 (1974).

[10] D. Dauvergne, C. Scheidenberger, A. L'Hoir, J. U. Anderson, S. Andriamonje, C. Böckstiegel, M. Chevallier, C. Cohen, N. Cue, S. Czajkowski, J. S. Forster, H. Geissel, H. Irnich, T. Kandler, R. Kirsch, A. Magel, P. H. Mokler, G. Münzenberg, F. Nickel, Y. L. Pivovarov, J. C. Poizat, M. F. Politis, J. Remillieux, D. Schmaus, T. Stöhlker, T. Suzuki, and M. Toulemonde, Phys. Rev. A **59**, 2813 (1999).

[11] B. R. Appleton, R. H. Ritchie, J. A. Biggerstaff, T. S. Noggle, S. Datz, C. D. Moak, H. Verbeek, and V. N. Neelavathi, Phys. Rev. B **19**, 4347 (1979).

[12] J. E. Miraglia, R. Gayet, and A. Salin, Europhys. Lett. **6**, 397 (1988).

[13] D. Dauvergne, A. Braüning-Demian, F. Bosch, H. Braüning, M. Chevallier, C. Cohen, A. Gumberidze, A. L'Hoir, R. Kirsch, C. Kozhuharov, D. Liesen, P. H. Mokler, J. C. Poizat, C. Ray, T. Stöhlker, M. Tarisien, E. Testa, S. Toleikis, and M. Toulemonde, Nucl. Instr. and Meth. B **205**, 773 (2003).

[14] F. Barrué, M. Chevallier, D. Dauvergne, R. Kirsch, J. C. Poizat, C. Ray, L. Adoui, A. Cassimi, H. Rothard, M. Toulemonde, C. Cohen, A. L'Hoir, D. Vernhet, C. Demonchy, L. Giot, W. Mittig, S. Pita, P. Roussel-Chomaz, and A. Billebaud, Phys. Rev. A **70**, 032902 (2004).

[15] A. Leon, S. Melki, D. Lisfi, J. P. Grandin, P. Jardin, M. G. Suraud, and A. Cassimi, At. Data and Nucl. Data Tables **69**, 217 (1998).

[16] H. Weick, H. Geissel, C. Scheidenberger, F. Attallah, D. Cortina, M. Hausmann, G. Münzenberg, T. Radon, H. Schatz, K. Schmidt, J. Stadlmann, K. Sümmerer, and M. Winkler, Phys. Rev. Lett. **85**, 2725 (2000).

[17] A. L'Hoir, S. Andriamonje, R. Anne, N. V. De Castro Faria, M. Chevallier, C. Cohen, J. Dural, R. Gayet, R. Genre, M. Hage-Ali, R. Kirsch, B. Farizon-Mazuy, J. Mory, J. Moulin, J. C. Poizat, Y. Quéré, J. Remillieux, D. Schmaus, and M. Toulemonde, Nucl. Instr. and Meth. B **48**, 145 (1990).

[18] A. L'Hoir, L. Adoui, F. Barrué, A. Billebaud, F. Bosch, A. Braüning-Demian, H. Braüning, A. Cassimi, M. Chevallier, C. Cohen, D. Dauvergne, C. E. Demonchy, H. Rothard, J. P. Rozet, T. Stöhlker, M. Tarisien, E. Testa, S. Toleikis, and M. Toulemonde, Nucl. Instr. and Meth. B **245**, 1 (2006).

[19] H. F. Krause and S. Datz, Adv. Atom. Mol. Opt. Phys. **37** (1996).

[20] G. Bednarz, A. Warczak, D. Sierpowski, T. Stöhlker, S. Hagmann, F. Bosch, A. Gumberidze, C. Kozhuharov, D. Liesen, P. H. Mokler, X. Ma, and Z. Stachura, Hyperfine Interaction **146/147**, 29 (2003).

[21] H. A. Bethe and E. E. Salpeter, *The Physics of One- and Two-Electron Atoms* (New York, 1977).
[22] F. Grüner, W. Assmann, F. Bell, M. Schubert, J. U. Andersen, S. Karamain, A. Bergmaier, G. Dollinger, L. Görgens, W. Günther, and M. Toulemonde, Phys. Rev. B **68**, 174104 (2003).
[23] E. Bonderup, H. Esbensen, J. U. Andersen, and E. Schiott, Rad. Eff. **12**, 261 (1972).
[24] E. Testa, D. Dauvergne, A. Braüning-Demian, F. Bosch, H. Braüning, M. Chevallier, C. Cohen, A. Gumberidze, A. L'Hoir, R. Kirsch, C. Kozhuharov, D. Liesen, P. Mokler, J. C. Poizat, C. Ray, J. P. Rozet, T. Stöhlker, S. Toleikis, M. Toulemonde, and P. Verma, Nucl. Instr. and Meth. B **245**, 47 (2006).
[25] T. Stöhlker, C. Kozhuharov, P. H. Mokler, A. Warczak, F. Bosch, H. Geissel, R. Moshammer, C. Scheidenberger, J. Eichler, A. Ichihara, T. Shirai, Z. Stachura, and P. Rymuza, Phys. Rev. A **51**, 2098 (1995).
[26] S. Andriamonje, M. Chevallier, C. Cohen, N. Cue, D. Dauvergne, J. Dural, F. Fujimoto, R. Kirsch, A. L'Hoir, J. C. Poizat, Y. Quéré, J. Remillieux, C. Röhl, H. Rothard, J. P. Rozet, D. Schmaus, M. Toulemonde, and D. Vernhet, Phys. Rev. A **54**, 1404 (1996).
[27] S. Andriamonje, M. Chevallier, C. Cohen, J. Dural, M. J. Gaillard, R. Genre, M. Hage-Ali, R. Kirsch, A. L'Hoir, B. Mazuy, J. Mory, J. Moulin, J. C. Poizat, J. Remillieux, D. Schmaus, and M. Toulemonde, Phys. Rev. Lett. **59**, 2271 (1987).
[28] J. P. Rozet (private communication).
[29] D. Belkic, R. Gayet, and A. Salin, Phys. Reports **56**, 279 (1979).
[30] W. Lotz, Z. Physik **216**, 241 (1968).
[31] K. Omidvar, At. Data and Nucl. Data Tables **28**, 1 (1983).